Magnetic decrease formation from <1 AU to ~5 AU: Corotating interaction region reverse shocks

Bruce T. Tsurutani,[1] Fernando L. Guarnieri,[2] Ezequiel Echer,[3] Gurbax S. Lakhina,[4] and Olga P. Verkhoglyadova[1,5]

Received 17 November 2008; revised 8 February 2009; accepted 13 May 2009; published 18 August 2009.

[1] Magnetic decreases (MDs) have been identified and studied throughout a Ulysses fast latitude scan that lasted from 29 February 1992 to 14 September 1993. Ulysses' distance was ~5 AU from the Sun. MDs were unbiasedly selected by application of the Interplanetary Magnetic Decrease Automatic Detection code. MDs were found to occur in high-occurrence-frequency "clusters" with the top 10 peak events varying in magnitude from 116 MDs per day to 36 MDs per day. For comparative purposes, quiet, nonpeak intervals had an occurrence rate of 4.3 MDs per day. Each of the 10 MD clusters was analyzed in detail to determine their solar wind dependences. MD clusters were often found to occur within corotating interaction regions (CIRs), mainly localized in the trailing portions of CIRs between the interface (IF) and the reverse shock (RS). The MD clusters were divided into smaller subclusters. Within the limits of this study, MD subclusters were always found to occur in high-β ($1 < \beta < 10^2$) regions (HBRs). Small MD subclusters were detected in HBRs downstream of forward shocks (FSs) but less frequently than for the trailing portion of the CIR. The FS to IF region is generally a low-β region (LBR), where $\beta \leq 1.0$. The 3920 MDs were identified in the study. The temporal thickness distribution of MDs is given by $N = 2173\ e^{-(t/17.3)}$, where t is in seconds. The magnetic field angular changes were calculated across MDs. The angular dependence is $\%MDs = 2 + 48e^{-(\Delta\Theta°/18.8°)}$. Only 13.5% of MDs were "linear" with angular changes <10° across the structures. Because MDs are found in abundance in the region spanning the CIR RS to close to the IF, it is argued that MDs must be formed continuously from close to the Sun (r < 0.5 AU) to ~5 AU. The older MDs (those found close to the IF) are "fossils" that have been convected radially outward to ~5 AU. A scenario is presented to explain the HBRs downstream of both CIR RSs and quasi-parallel FSs. The location of MD clusters in the trailing parts of CIRs and the paucity of linear MDs indicate that MD generation by mirror mode instability is unlikely. More promising candidates are shock compression of phase-steepened Alfvén waves, shock–directional discontinuity interactions, and downstream turbulence. We emphasize the phase-steepened Alfvén wave mechanism.

Citation: Tsurutani, B. T., F. L. Guarnieri, E. Echer, G. S. Lakhina, and O. P. Verkhoglyadova (2009), Magnetic decrease formation from <1 AU to ~5 AU: Corotating interaction region reverse shocks, *J. Geophys. Res.*, *114*, A08105, doi:10.1029/2008JA013927.

1. Introduction

[2] Magnetic decreases (MDs) (also called magnetic holes or MHs) have been defined as abrupt, >50% decreases in the interplanetary magnetic field magnitude [*Turner et al.*, 1977; *Winterhalter et al.*, 1994; *Tsurutani and Ho*, 1999; *Fränz et al.*, 2000; *Neugebauer et al.*, 2001; *Stevens and Kasper*, 2007]. The scale sizes range from 2 to 3 proton gyroradii to thousands of gyroradii or more. MDs are ubiquitous features in the interplanetary medium and are an important component of "compressional" heliospheric turbulence.

[3] *Winterhalter et al.* [1994], *Tsurutani and Ho* [1999], and *Stevens and Kasper* [2007] have speculated that MDs are created close to the Sun and the "fossil structures" are convected to 1 AU and beyond. On the other hand, *Tsurutani et al.* [2005a, 2005b] have found evidence that some MDs are being created just upstream of the Earth (between ACE and Cluster) by an Alfvén wave phase-steepening process.

[4] It is the purpose of this paper to analyze Ulysses magnetic field and plasma data during a fast latitude scan

[1]Jet Propulsion Laboratory, California Institute of Technology, Pasadena, California, USA.
[2]Instituto de Pesquisa e Desenvolvimento, Universidade do Vale do Paraíba, São José dos Campos, Brazil.
[3]Instituto Nacional Pesquisas Espaciais, São José dos Campos, Brazil.
[4]Indian Institute of Geomagnetism, Navi Mumbai, India.
[5]Center for Space Plasma and Aeronomic Research, University of Alabama in Huntsville, Huntsville, Alabama, USA.

0148-0227/09/2008JA013927

that occurred from 14 September 1992 to 12 September 1993 at a distance of ~5 AU from the Sun. The causes of the high occurrence rates of MDs at low to medium heliographic latitudes previously noted by *Winterhalter et al.* [2000] and *Tsurutani et al.* [2005a] will be studied in detail. A new code called the Interplanetary Magnetic Decrease Automatic Detection (IMDAD) routine [*Guarnieri et al.*, 2009] will be used to identify the MD events. It will be shown that some MDs are being created locally at ~5 AU and others are convected fossils that have come from distances closer to the Sun. Our analyses will identify solar wind conditions that are conducive for MD formation. Solar wind regions where MDs are not found are also identified. In conclusion, we will discuss the results in light of various proposed MD generation mechanisms.

2. Theoretical Background

[5] There are at least six major proposed mechanisms for MD formation in interplanetary space: (1) mirror instability [*Winterhalter et al.*, 1994, 1995; *Stevens and Kasper*, 2007], (2) shock–directional discontinuity (DD) interactions [*Tsubouchi and Matsumoto*, 2005], (3) wave-wave interactions/turbulence [*Vasquez et al.*, 2007; *Tsubouchi*, 2007], (4) soliton formation [*Baumgärtel*, 1999], (5) nonlinear Alfvén wave evolution [*Buti et al.*, 2001], and (6) Alfvén wave phase steepening [*Tsurutani et al.*, 1994, 2002a, 2002b, 2003, 2005a, 2005b].

[6] The conditions for the onset of the mirror instability (mechanism 1) are that $\beta_\perp/\beta_\parallel > 1 + 1/\beta_\perp$ [*Chandrasekhar et al.*, 1958; *Hasegawa*, 1969, 1975; *Price et al.*, 1986; *Brinca and Tsurutani*, 1988; *Pokhotelov et al.*, 2004, 2005; *Shoji et al.*, 2009], where $\beta_\perp$ and $\beta_\parallel$ are the perpendicular and parallel plasma beta values (the plasma β is the ratio of plasma thermal pressure to magnetic pressure). Quasi-perpendicular shock compression of upstream plasma will heat the plasma preferentially in the $T_\perp$ direction. It has been speculated that this compression could potentially lead to mirror mode structure/linear MD generation (linear MDs have been defined by *Burlaga and Lemaire* [1978] and *Winterhalter et al.* [1994] as those MDs where there are only small angular changes (<10°) in the magnetic field directionality during the events). This potential mechanism will be discussed further later in this paper.

[7] It has recently been postulated that DDs interacting with compressive shocks can lead to rapid MD formation/evolution (mechanism 2). *Tsubouchi and Matsumoto* [2005] have modeled plasma interactions with DDs immediately downstream of the Earth's bow shock with resultant MD formation (confirmed by data from the event). In their simulation, proton parallel heating occurs from enforced conversion of proton perpendicular motion into parallel motion by the imposed rotational magnetic field. The resultant intense parallel/antiparallel flows are believed to generate the field gradient at the edges, acting as a mirror force reducing the magnetic intensity.

[8] *Vasquez et al.* [2007] have suggested wave-wave interactions (mechanism 3) in the turbulent sheaths behind interplanetary shocks could create MDs. *Tsubouchi* [2007] have suggested a slightly different wave-wave interaction mechanism. Reflection of Alfvén waves (AWs) from shocks will lead to AW-AW interactions, which in some instances may lead to MD formation. These MDs would be swept downstream into the sheath region behind the shock.

[9] *Baumgärtel* [1999] has proposed a model (mechanism 4) in which the MDs arise from the rarefractive MHD soliton solutions of the derivative nonlinear Schrödinger equation (DNLS [*Kennel et al.*, 1988]) governing Alfvén wave propagation at small angles to the ambient magnetic field. However, use of DNLS for studying the evolution of Alfvén waves propagating at large angles is questionable.

[10] *Buti et al.* [2001] have proposed a model (mechanism 5) where the evolution of large-amplitude right-hand-polarized Alfvénic wave packets propagating at large angles to the magnetic field can generate MDs in the solar wind. In this model, the presence of proton thermal anisotropy is favorable, but not necessary, for the generation of MDs.

[11] *Tsurutani et al.* [2002a, 2002b, 2005a] have proposed that MDs are generated owing to a diamagnetic effect of perpendicularly heated (relative to the magnetic field B_o) protons (mechanism 6). The mechanism for proton heating is the Ponderomotive Force associated with phase-steepened edges (rotational discontinuities) of interplanetary Alfvén waves [*Dasgupta et al.*, 2003].

3. Method of Analyses

[12] A new code, called the Interplanetary Magnetic Decrease Automatic Detection (IMDAD) code, has been used to identify the beginnings and ends of MDs. This code is described in detail by *Guarnieri et al.* [2009]. The criterion for MD selection used in this study is $B_{min} < 0.5\ B_0$. The code parameters used have a sliding window of 300-s width and were applied to Ulysses 1-s high-time-resolution magnetic field data. IMDAD avoids double counting of MDs closer together than 30 s.

[13] *Winterhalter et al.* [2000] and later *Tsurutani et al.* [2005a] noted greater MD occurrence rates during the Ulysses 1992–1993 fast latitude scan where many corotating streams were present. Because of this previous finding, this interval will be examined in greater detail to determine what specific interplanetary feature or features are responsible for the large MD occurrence rates found near the ecliptic plane. Determination of this feature or features will place important constraints on the physical mechanisms forming MDs in interplanetary space.

4. Results

4.1. IMDAD Selection Examples

[14] Figure 1 is an example of the IMDAD selection of MDs during a high-speed stream interval with large-amplitude Alfvén waves present. The interval is on day 344, 1992, from 344.2 to 344.8 (and is event 7 in Figure 3). The magnetic fields are given in the interplanetary RTN coordinate system. In this system, R points radially outward from the Sun toward the spacecraft, T is $\Omega \times R/|\ \Omega \times R\ |$, where Ω is the north solar rotation pole, and N completes the right-hand system. The beginning and end of the MDs are indicated by a dotted vertical line and a dashed vertical line, respectively.

[15] Most of these MDs are of short duration. Many MDs are associated with sharp rotations of the interplanetary magnetic field (IMF). Examples can be noted at ~344.25,

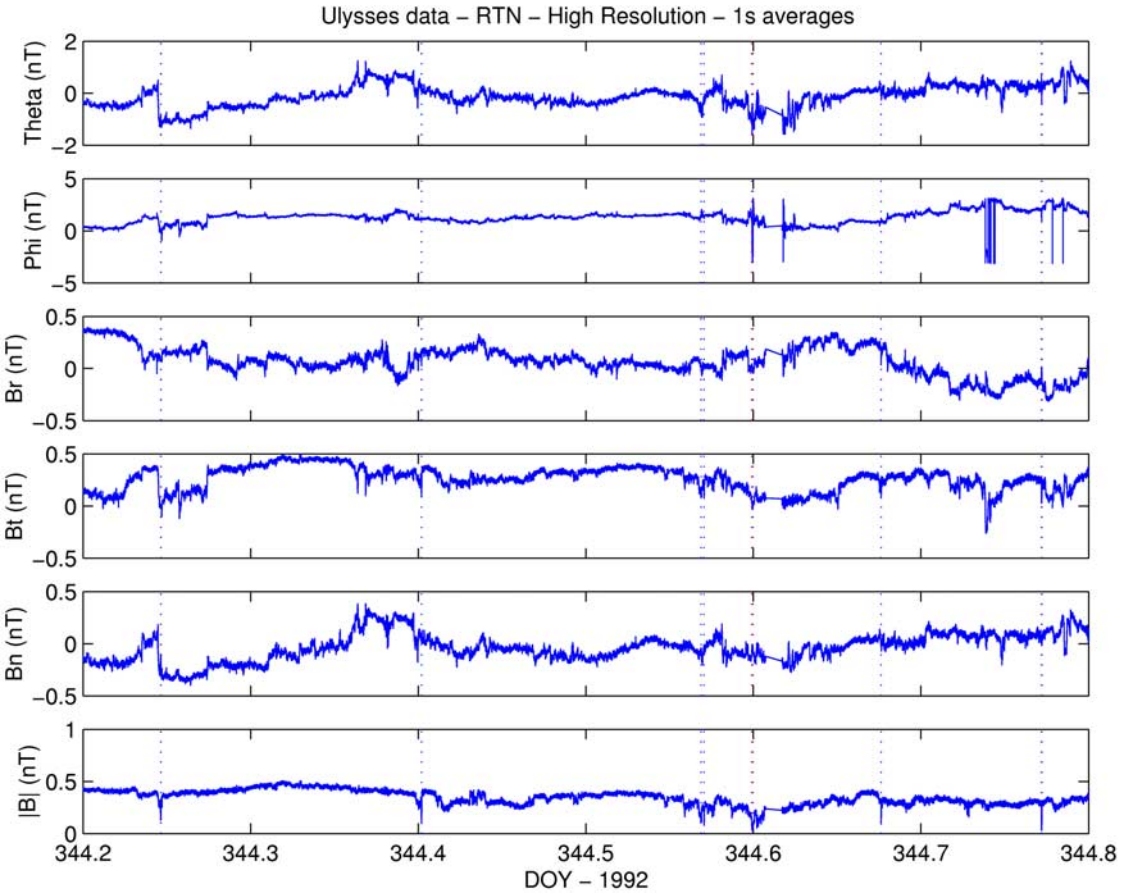

Figure 1. Examples of MD start and stop times identified by the Interplanetary Magnetic Decrease Automatic Detection (IMDAD) code. These events occurred in a high-speed stream during day 344, 1992.

~344.40, and ~344.60. These events may be caused by the Alfvén wave phase-steepening mechanism [*Tsurutani et al.*, 2005a, 2005b] or other nonlinear wave effects [*Buti et al.*, 2001].

[16] Figure 2 is another interval with MDs identified by IMDAD. This time interval extends from day 96.715 to day 96.740, 1993. This interval also occurred during a high-speed stream (stream 11 in Figure 3). These MDs have a different nature. There are little or no angular changes before, during, and after the MDs. These have been called "linear holes" by *Winterhalter et al.* [1994] following the thought that mirror mode (MM) structures [*Tsurutani et al.*, 1982, 1995, 1999] have little or no angular change across them. Examples of linear holes can be found approximately at day 96.727, day 96.729, etc.

4.2. MD Occurrence Rate Spikes/Clusters

[17] Figure 3 shows 1992–1993 Ulysses fast latitude scan data. The interval begins at 29 February 1992 and ends on 14 September 1993. Figure 3 contains the solar wind velocity and the number of MDs per day. Major corotating streams are numbered sequentially from 1 to 16. This numbering is the same as that used by *Bame et al.* [1993] and *Smith et al.* [1993]. The streams occur at ~25-day intervals. During this interval, Ulysses moved from the equatorial plane toward the south polar region. It should be noted that the interval that we study here is somewhat larger than that studied by *Bame et al.* [1993] and *Smith et al.* [1993]. The latter authors focused primarily on the corotating stream interval.

[18] The number of MDs per day can be noted to be highly anisotropic. There are numerous large MD occurrence rate spikes. The 10 largest spikes within the interval have been identified and are labeled in order of descending magnitude. These will be hereinafter referred to as MD events 1, 2, etc. Two of the largest spikes, MD events 1 and 7, occur prior to the high-speed corotating stream interval. The other events are present primarily between high-speed streams 6 and 16. Because MDs are often concentrated together, we will refer to these occurrence rate spikes as clusters.

[19] MD event 1 (by definition the largest MD cluster) had 116 MDs per day, and event 10 had 36 MDs per day. There are days where there are little or no MDs as well. If the 10 largest MD peaks are removed from the data set, the remaining "background" level is 4.3±6.1 MDs per day. These 10 large peaks have intensities much greater than statistical fluctuations can account for.

4.3. MDs and Corotating High-Speed Streams

[20] Although Figure 3 may appear to show a very simple picture of one major corotating high-speed stream appearing

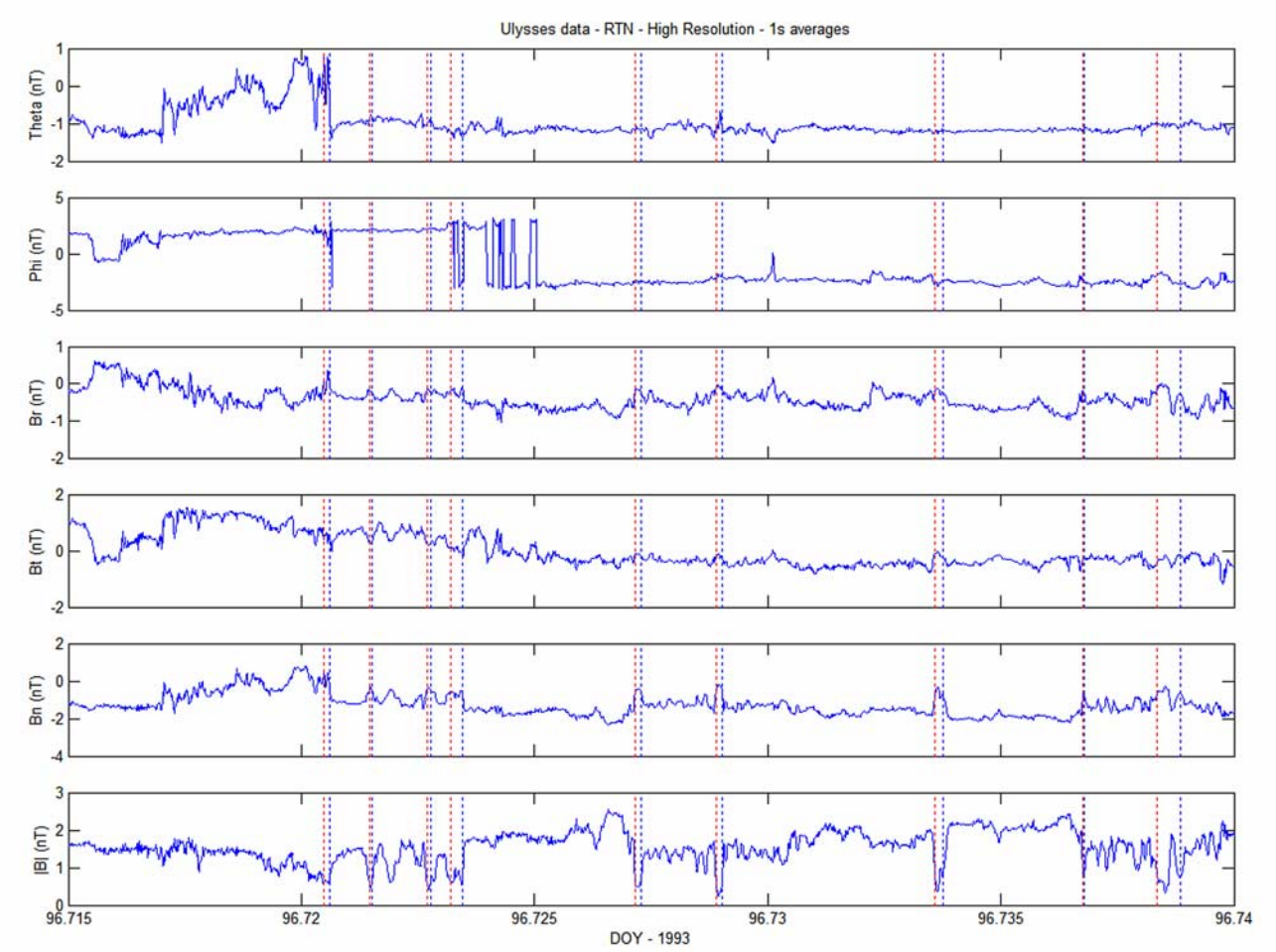

Figure 2. Same as Figure 1 but during day 96, 1992. These MDs were detected within a high-speed stream.

over and over again at a ~25-day recurrence period, in actuality the structures were far more complex (see discussion in the work of *Smith et al.* [1993]). Figure 4 shows part of this interval in higher time resolution. Figure 4 contains some of the same data as that given in Figure 3, but the magnetic field magnitude has been added (in blue). There are four major corotating interaction regions (CIRs) found for each solar rotation period. These are labeled as "a," "b," "c," and "d" events. The labeling scheme that we use follows that of *Smith et al.* [1993], based on visual inspection. The major (largest magnitude) CIRs are the d events for most of the stream events. The CIR d event is present at the leading edge of the high-speed stream events 9, 11, and 12 (there is a data gap at event 10, so the relationship there is unclear). These CIRs are bounded by forward and reverse shocks. The details of the shock properties are given by E. Echer et al. (Forward and reverse shocks at 4–5 AU, submitted to *Advances in Space Research*, 2009). The d event was much smaller in the region between streams 12 and 13 as Ulysses went to lower southern latitudes. A d event is also present at the leading edge of stream 8 but was not identified by *Smith et al.* [1993].

[21] There is a strong relationship between MDs and the CIR d events. This can be noted at stream 8 (MD event 3), a 34 MDs per day peak at stream 9, MD event 5 at stream 10, a 31 MDs per day event peak at stream 11, and the MD event 4 in stream 12. For the small CIR d event between streams 12 and 13, there are very few MDs.

[22] It should also be noted that there are large MD peak occurrences that are not obviously associated with CIR d events. Events 1 and 2 are two obvious cases. These will be discussed separately.

[23] The lowest MD occurrence rates are found either near the peak speeds of the high-speed streams or in the declining speed regions. This can be clearly noted from all of the stream events from 8 through 13. Figures 1 and 2 were examples of MDs observed in the high-speed stream proper, in these low MD occurrence rate regions.

4.4. MD Event 3

4.4.1. CIR Trailing Portions: MD Clusters, Subclusters, and High-β Regions

[24] The third most intense MD occurrence rate peak is displayed in Figure 5. The format and color coding is the same as that in Figure 4. This event spans 2 days. The peak MD occurrence rates are 56 and 67 events per day on days 363 and 364, 1992, respectively. The total number of MDs is thus 123 events, higher than the MD event 1. This is the

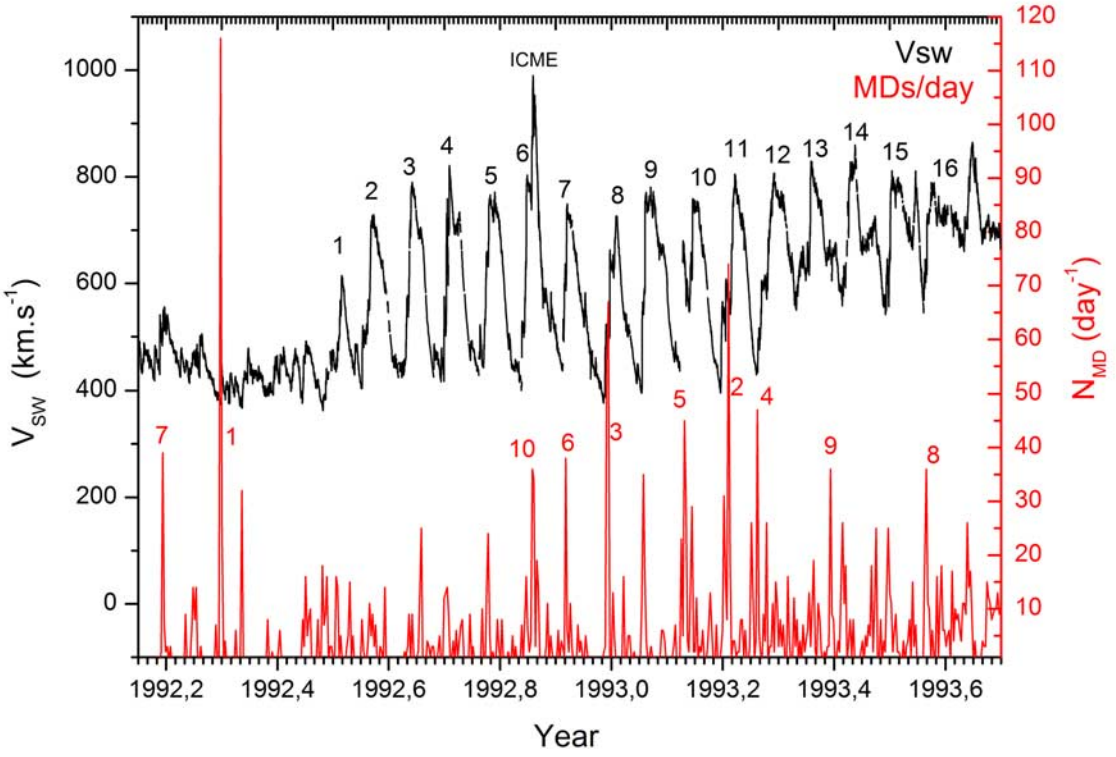

Figure 3. Ulysses fast latitude scan interval during 1992–1993. The sequence of fast solar wind streams is numbered according to the work of *Bame et al.* [1993] and *Smith et al.* [1993]. The number of MDs per day is given with the top 10 peaks in MD occurrence rate indicated.

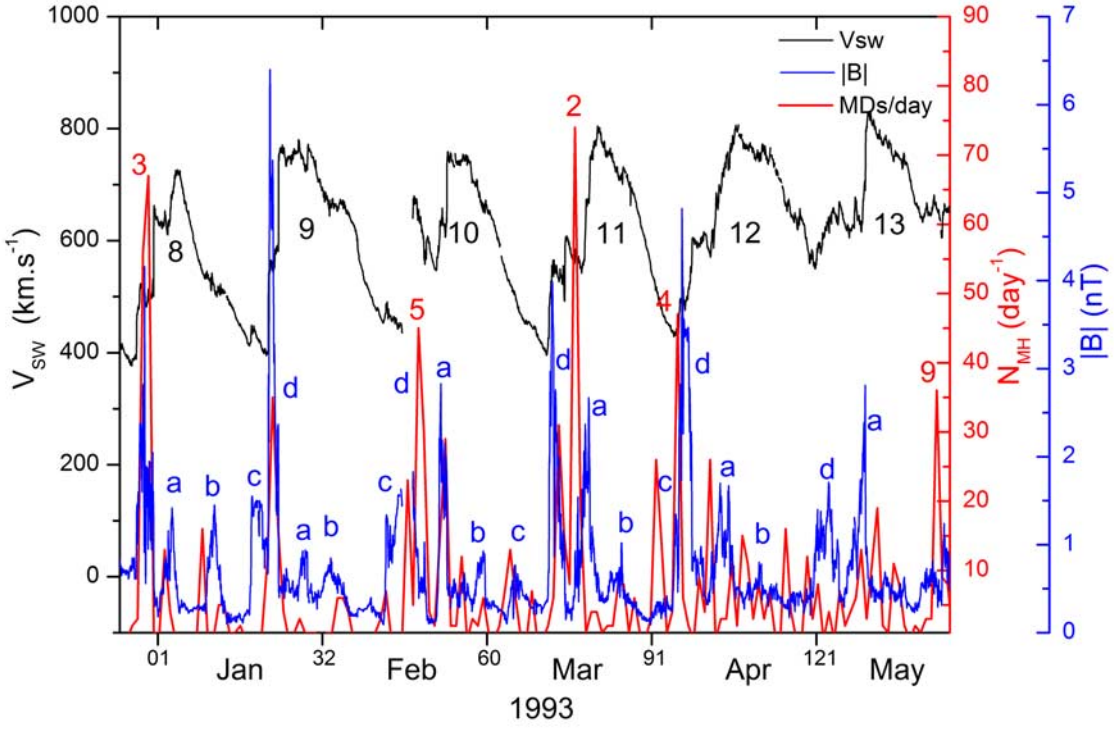

Figure 4. High-speed streams 8–11 are shown in higher time resolution. Also shown is the magnetic field magnitude. The CIRs are labeled according to the work of *Smith et al.* [1993]. This interval is quite complex.

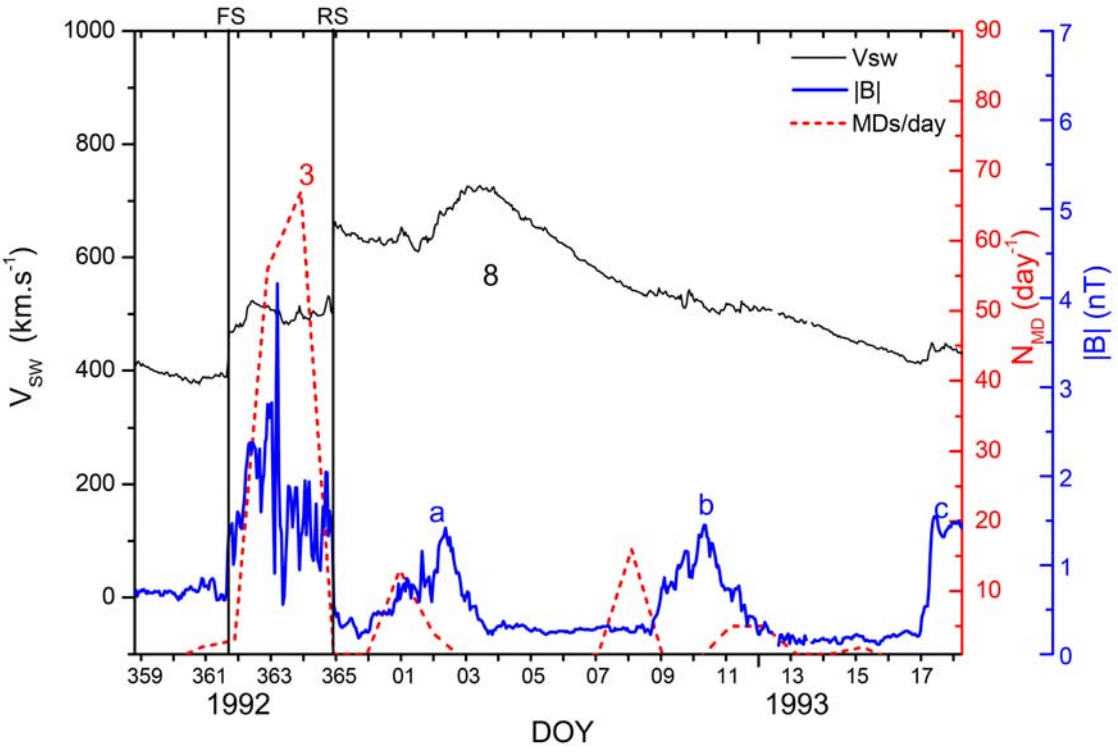

Figure 5. Stream 8 and MD cluster 3. MD cluster 3 occurred within a CIR over a 2-day interval.

CIR d event of high-speed stream 8. Note that the CIR is bounded by fast forward and fast reverse shocks.

[25] Figure 6 shows days 363–364, 1992, the CIR d event in high resolution. From top to bottom, the panels show the solar wind speed, proton density, proton temperature, and the magnetic field in the RTN coordinate system. The eighth and ninth panels show the magnetic field polar θ and φ angles (defined in the standard sense). The forward shock is present at approximately day 361.8 (26 December 1992), and the reverse shock is near day 365.0 (~0000 UT, 30 December 1992). The shocks are indicated in Figure 6 by vertical dashed lines. At approximately day 363.3–363.4, there are sharp discontinuities in the density, temperature, and B magnitude. This is the CIR interface (IF), the discontinuity that separates the shocked slow-speed stream plasma from the shocked high-speed stream plasma. The magnetic field φ angle switches from $\sim -90°$ to $\sim +90°$ from 363.1 to 363.4, indicating a crossing of the heliospheric current sheet (HCS). The HCS [*Smith et al.*, 1978] is thus embedded in this CIR structure.

[26] Figure 7 is the same event as that in Figure 6 but with the individual MDs indicated by vertical dashed lines. Only the MD onset times are indicated to simplify Figure 7. The first through seventh panels show the solar wind plasma and field parameters. The eighth panel shows the plasma β.

[27] An obvious feature of Figure 7 is that the MD occurrence rate is highly asymmetric relative to the CIR. There are very few events between the forward shock (FS) and the interface (IF). Most MDs are found in the region between the IF and the reverse shock (RS). The MDs are thus found to be "clustered" together. The 2-day MD cluster (MD event 3, Figure 5) occurs on days 363 and 364, primarily in the latter region.

[28] Although the high MD occurrence rates from day ~363.2 to day 365.0 can be considered a broad cluster, there are lots of substructures within this event. We will refer to these as "subclusters." There are two MD subclusters that occur close to the IF, one at day 363.2, 1992, antisunward of the IF (between the FS and the IF), and another at day 363.5, 1992, sunward of the IF (between the IF and the RS). Since plasma near the IF is the oldest within the CIR (plasma and magnetic fields are accumulated from outside the CIR (flowing through the FS and RS), these MD subclusters are associated with plasma processes that originated close to the Sun (<1.0 AU).

[29] The two MD subclusters noted above occur in very high β plasma regions, $10^1 < \beta < 10^2$. These two regions (hereinafter called high-β regions, or HBRs) have the highest β values for the entire CIR. The magnetic field magnitudes within these HBRs are quite low (<1 nT) and are also highly variable. This variability leads to a "hashy-like" appearance. The latter two features are typical of HBRs studied in this effort.

[30] There are many other subclusters that occur between day 363.7 and day 365.0. The MDs are almost always detected in intervals where $1 < \beta < 10^1$. None of the tens of MDs were detected when $\beta < 1.0$.

[31] Two other MD subclusters are particularly noteworthy. In the leading portion of the CIR, at ~362.0, there is a small MD subcluster. This occurs in a region where $\beta > 1.0$. This subcluster is just downstream of the FS (approximately day 361.8). A second MD subcluster which occurs at ~364.8 is similar in nature. It occurs in a $\beta > 1.0$ interval and is just downstream of the RS (day 365.0). These MD subclusters, which are located downstream of but close to the shocks, must have been formed recently (at ~5 AU).

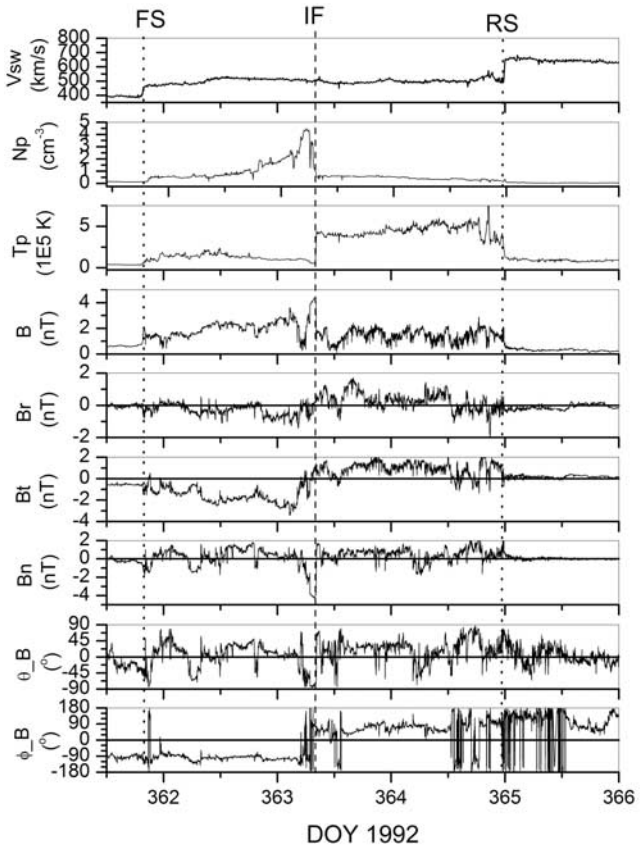

Figure 6. A high-resolution image of CIR 2, the event in Figure 5. The forward shock (FS), reverse shock (RS), and interface (IF) are noted.

[32] Other MD occurrence rate peaks/clusters have been examined. The clusters were composed of subclusters. The subclusters were related to HBRs. This relationship was found to be true for the events examined in this study.

4.4.2. Leading Portions of CIRs: Low-β Regions and an Absence of MDs

[33] In Figure 7, for the interval from 362.1 to 363.2 within the CIR leading edge, there is only 1 MD present. In this region, $\beta \sim 1.0$. The magnetic field magnitude is relatively high (1–2 nT), and it varies smoothly with time. This is characteristic of the low-β regions (LBRs) examined in this study.

[34] There are also small regions of low-β plasma in the trailing part of the CIR. At ~363.7 and ~364.5, $\beta \sim 1.0$. These are regions without MDs.

4.5. MD Event 2: Association With a Small Solar Wind Stream

[35] The second most intense MD occurrence rate peak (MD event 2) is shown in detail in Figure 8. It can be noted that high-speed stream 11 is actually composed of many superposed streams that lead to the creation of the d, a, and b CIRs. This is true for many of the high-speed stream events discussed previously.

[36] Coincident with MD event 2 is a very small solar wind velocity increase at ~2350 UT day 76, 1993. *Abraham-Shrauner*'s [1972] plasma and magnetic field shock normal technique and Rankine-Hugoniot calculations were applied. The leading edge of this event has been identified as a forward shock. The shock normal angle is $\theta_{AS} \sim 80°$, and the magnetosonic Mach number $M_{ms} = 2.7$ (see Echer et al. (submitted manuscript, 2009) for details). This is a quasi-perpendicular forward shock at the time of crossing.

[37] The details of this small CIR are shown in Figure 9. The shock is identified by a vertical black line. It is noted that in the upstream region, the largest magnetic field component is the B_R component (B_T and B_N are both ~0 nT). There are foreshock waves present from day 76.7 to the shock at day 77.0. Thus one interpretation of the presence of upstream waves is that the waves may have strongly influenced the instantaneous nature of this shock. The shock may have been a quasi-parallel one in the past.

[38] The MDs are indicated by vertical dashed lines. The event 2 MD cluster occurred on day 77. The majority of MDs are found in the downstream sheath region from day 77.07 to day 77.4 and from day 77.58 to day 77.75. These latter two regions correspond to HBR/low magnetic field magnitude regions, similar to the results shown in Figure 7. MDs occur in $1 < \beta < 10^2$ regions.

[39] There are also low-β ($\beta < 1$) plasma regions in this interval. Two regions in Figure 9 are from day 77.0 to day 77.08 and from day 77.4 to day 77.58. These regions are devoid of MDs.

4.6. MD Event 1: Association With an FS

[40] MD event 1 is shown in high resolution in Figure 10. The Ulysses 1-s data are displayed in RTN coordinates and the MD onset times are indicated by the vertical dashed lines. A forward shock occurred at ~1715 UT day 109, 1992. Calculations determined that this shock was oblique ($\theta_{AS} = 44°$) in nature with a magnetosonic Mach number $M_{ms} = 3.1$. This shock also has upstream, non-compressive foreshock waves present between days 109.5 and 109.6 and farther upstream. We refer the reader to the work of *Gonzalez-Esparza et al.* [1996] for more details concerning the upstream waves ahead of the oblique/quasi-parallel shock. *Gonzalez-Esparza et al.* [1996] have argued that this FS is at the leading antisolar edge of a CIR.

[41] The MDs occurred in the sheath downstream of the FS. The MDs were related to high-plasma-β ($1 < \beta < 10^2$) regions. The magnetic field magnitude was weak, <0.5 nT. These results are similar to those of the MD subclusters for MD events 3 and 2.

4.7. The 10 Largest MD Occurrence Rate Spikes/Clusters

[42] MD cluster events 3, 6, 7, and 8 have the classic relationship between well-developed CIRs and MD clusters. The MD occurrence rate is highest in the trailing portion of the CIR, between the IF and RS. MDs are detected in HBRs where the magnetic field magnitudes are very low and have hashy appearances. There is a general lack of MDs in the LBRs between the FS and the IF.

[43] MD event 2 is associated with a small high-speed stream led by a quasi-perpendicular FS. However, the upstream field orientation and the presence of foreshock waves indicate that the shock normal may be highly variable. Event 5 occurs in a "ledge" behind a CIR proper. It is not certain what this region corresponds to at this time.

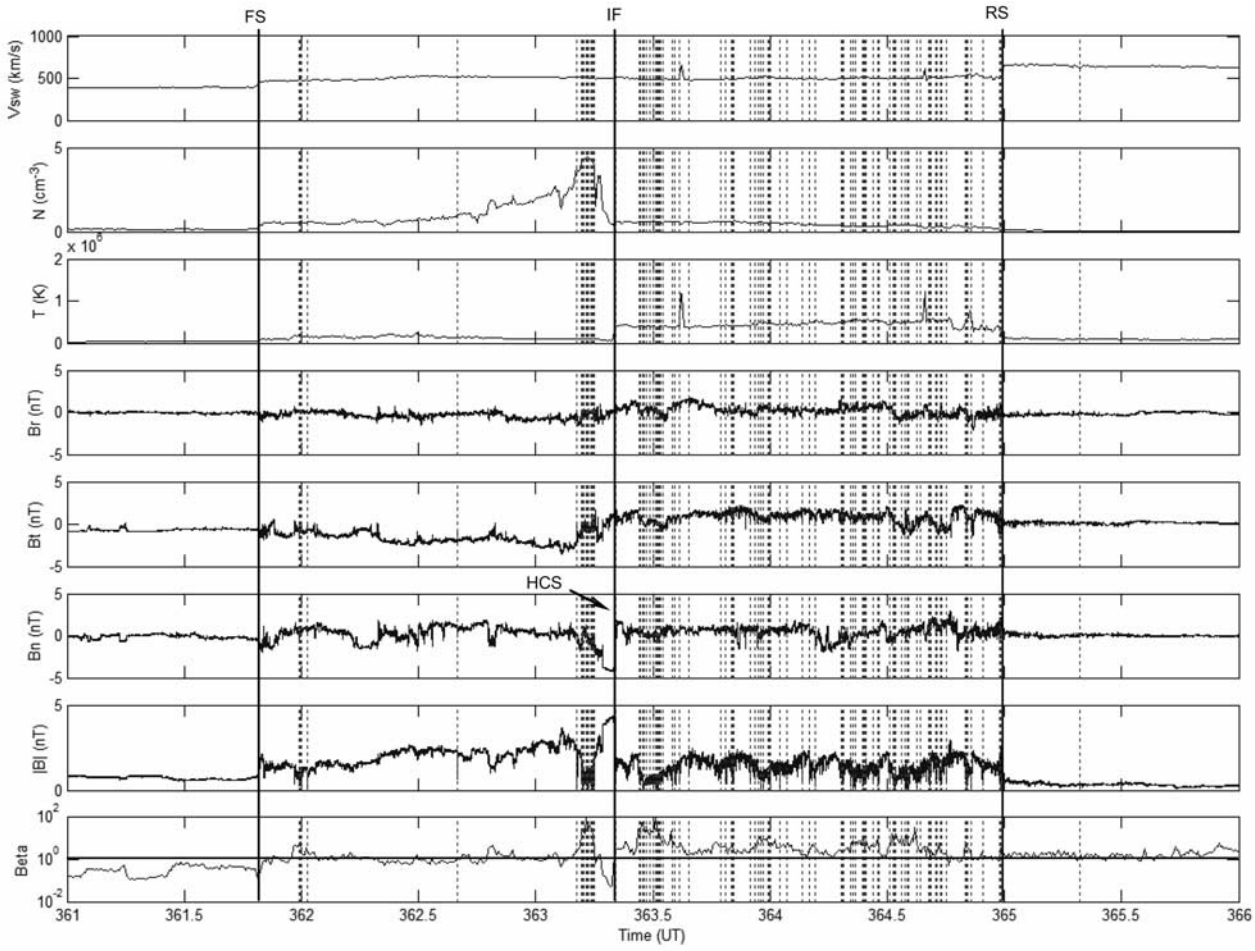

Figure 7. The same CIR event in Figures 5 and 6 with MD onsets indicated by vertical dashed lines. There is a general lack of MDs in the interval between the FS and the IF. Almost all MDs are detected between the IF and the RS. The rate of occurrence of MDs inside the CIR is much higher than in the high-speed stream proper (Figures 1 and 2).

Further investigation will be required to resolve this issue. MD event 10 is associated with an interplanetary coronal mass ejection (ICME) sheath and occurs behind an HCS event.

[44] MD event 1 occurred downstream of an oblique FS. Upstream foreshock waves were present. The MD cluster was located in the sheath downstream of the shock.

4.8. Temporal Thicknesses of MDs

[45] The IMDAD program identifies the beginning and end of all MDs. In the interval of study, 3920 MDs were identified. The MD "temporal thicknesses" were calculated. The results are shown in histogram format in Figure 11. The number of MDs decreases with increasing thickness. This general result is consistent with those of previous studies [*Tsurutani and Ho*, 1999; *Stevens and Kasper*, 2007].

[46] The MD thickness distribution was fitted by power law and exponential curves. The results are shown in Figures 12a and 12b, respectively. The parameter fits are given in each part. The exponential fit is the better of the two results. The number of MDs can be given as $N = A_1\, e_1^{-(t/t)}$, where $A_1 = (2173 \pm 35)$ and $t_1 = 17.3$ s.

4.9. Angular Changes Within MDs: Linear Holes?

[47] The magnetic field angular change across a MD is important to determine whether it is linear [*Burlaga and Lemaire*, 1978; *Winterhalter et al.*, 1994, 1995] or not. *Winterhalter et al.* [1994] have used a cutoff of 10° as the definition of a linear MD. This same criterion will be used here.

[48] The maximum angular change (Θ) across a MD has been calculated relative to the magnetic field angle at the start of the MD. The percent occurrence of the angular changes is displayed in Figure 13 in histogram format. All of the 3920 MDs are represented. An exponential fit has been made to the date, neglecting the first bin (0°–10°). A fit of $\%MDs = 2 + 48e^{-(\Delta\Theta^\circ/18.8^\circ)}$ is found. Note that the curve does not go to zero at 180°.

[49] Of the MDs identified in this study, 13.5% are linear, with $\Theta \leq 10°$. Most (86.5%) MDs are not linear. This is in agreement with *Winterhalter et al.*'s [1994] results.

5. Summary of Observations

[50] We have identified MDs by applying the IMDAD code analyzing over ~1.5 years of Ulysses fast latitude scan

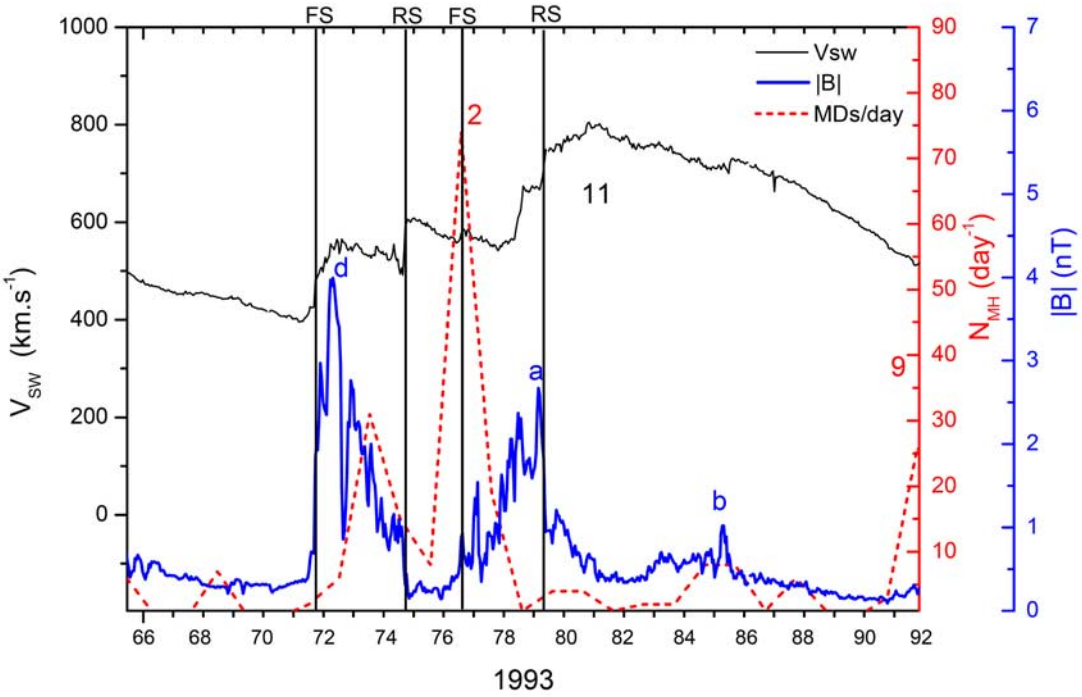

Figure 8. MD event 2 occurring close to high-speed stream 11.

high-resolution magnetic field data. The data interval spanned from $-5°$ at 5.4 AU to $\sim -35°$ at 4.5 AU, where $\sim$16 major (and many minor) high-speed streams and some ICME events were detected. The MD occurrence rates were highly variable, and the peak rates were well beyond statistical fluctuations. Below are some of the major findings.

5.1. Statistics

[51] 1. The top 10 MD events had an occurrence rate ranging from 116 MDs per day (event 1) to 36 MDs per day (event 10). The nonpeak average was 4.6 ± 6.7 MDs per day. The lowest MD occurrence rates were found at either the peaks or declining portions of the high-speed streams.

[52] 2. MDs have a wide range of temporal thicknesses. For the 3920 MDs detected, a $N = 2173e^{-(t/17.3)}$ distribution was determined.

[53] 3. Only 13.5% of MDs had angular changes <10° across the structures (linear MDs). The angular change dependence is $\%MDs = 2 + 48e^{-(\Delta\Theta°/18.8°)}$.

5.2. CIR Dependences

[54] 1. Half of the top 10 MD occurrence rate peaks were associated with CIRs. The MD occurrence within CIRs was highly asymmetric, with most of the MDs located in the trail part of the CIRs, between the interface (IF) and the reverse shock (RS).

[55] 2. The MD clusters were often composed of subclusters. The subclusters occur in small HBRs with $1 < \beta < 10^2$.

[56] 3. The leading (antisolar) portions of CIRs are typically low-β regions (LBRs) with $\beta < 1.0$. MDs are generally absent in these regions.

5.3. Forward Shocks and MDs

[57] Several sheaths downstream of ICME or CIR forward shocks contained MD clusters. For these cases, foreshock waves existed upstream of the shocks, indicating that they could be or have been quasi-parallel in nature. Similar to the CIR cases, the MD clusters contained subclusters. The MD subclusters occurred in HBRs with $1 < \beta < 10^2$.

6. Scenario for CIR High-β Structures

[58] To better understand both the regions where MDs occur and are absent, we first try to explain why there are HBRs and LBRs within CIRs. Figure 14 shows a schematic of a CIR in the ecliptic plane at large distances from the Sun (see also discussion by *Pizzo* [1985]). The antisolar edge is led by a forward shock (FS), and the trailing solar edge is bounded by a reverse shock (RS). The region between the FS and IF is shocked, accelerated slow solar wind plasma and fields, and the region between the IF and the RS is shocked, decelerated fast solar wind plasma and fields. The former is shown in blue in Figure 14 to indicate the lower solar wind temperatures and β values.

[59] The interplanetary magnetic fields are illustrated in Figure 14 by the black curved lines which indicate their Parker spiral configurations. The field in front of the FS is more curved owing to the slower speed of the slow solar wind (typically 300–400 km/s). The solar wind speed behind the RS is faster (500–700 km/s) and the magnetic fields are therefore more radial (from the Sun) than the fields upstream of the CIR. Thus, on average, the RS is statistically more quasi-parallel than the FS.

[60] Plasma and field compression (heating) is significantly different at quasi-perpendicular shocks than at quasi-parallel shocks. At a quasi-perpendicular shock, the plasma is preferentially heated perpendicular to the magnetic field; that is, the downstream plasma distribution will be heated in $T_\perp$. The magnetic field magnitude $|B_o|$ will be compressed

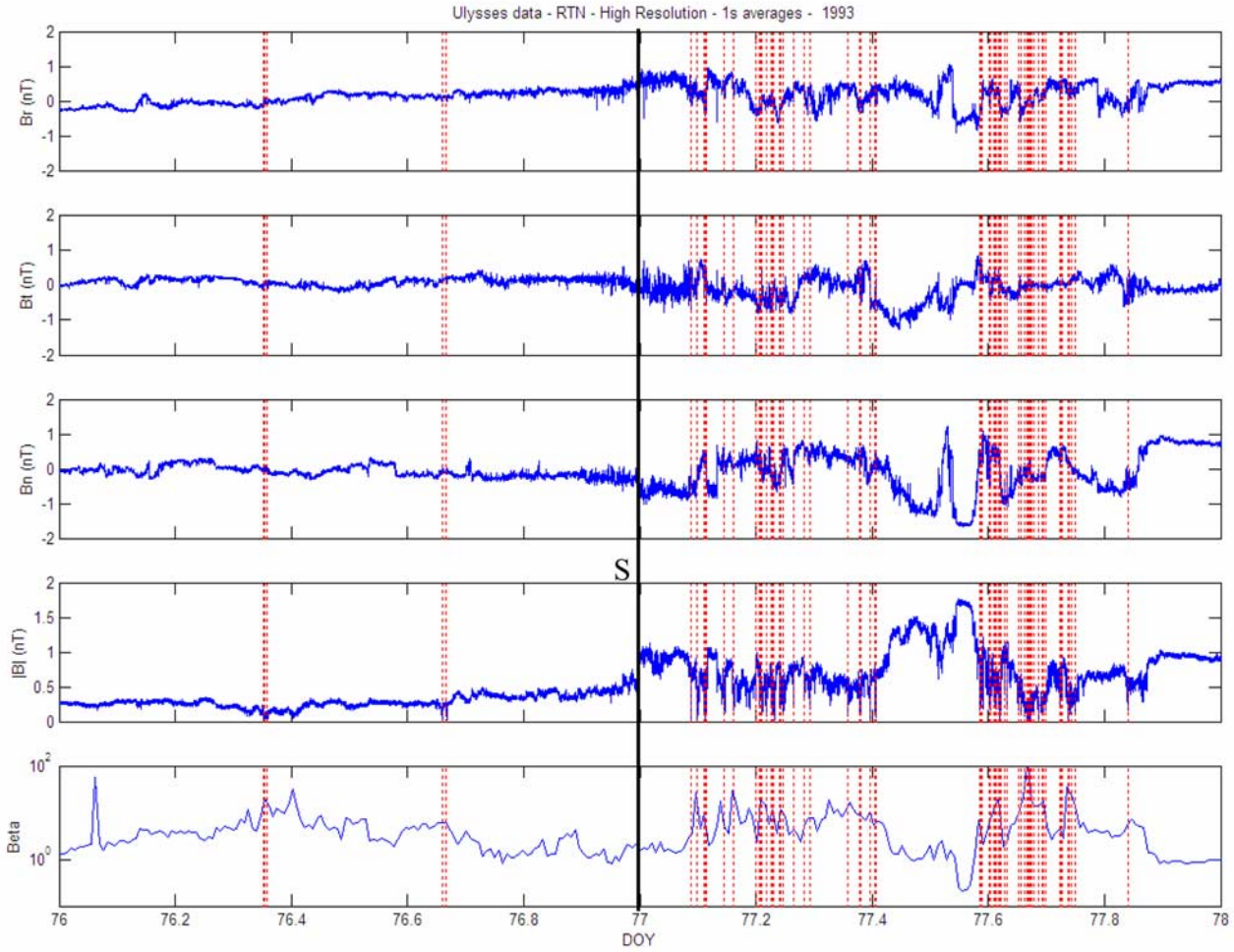

Figure 9. A high-resolution plot of MD event 2. The shock is indicated by a vertical black line. MDs are indicated by vertical dashed lines.

as well. For quasi-parallel shocks, the plasma will be heated parallel to the magnetic field. However, one major difference is that the magnetic field will be only slightly compressed. For the latter case, the downstream sheath plasma will become high-plasma-β regions. Thus the upstream magnetic field geometry and the nature of the FS and RS lead to significantly different downstream (CIR) plasma β conditions.

[61] Figure 14 gave a rough schematic of a CIR. A more realistic schematic is given in Figure 15. The black region in the center of the CIR designates the IF, separating the upstream region from the downstream region. Here both the antisolar part and the solar part of the CIR are shown to have many layers, owing to varying upstream conditions over time. The magnetic field directions within the CIR are indicated by the parallel stripes within the layers.

[62] In Figure 15, the LBR regions are blue, and the HBRs are red (or pink). Deep blue indicates strong LBRs ($\beta \ll 1.0$), and bright red indicates strong HBRs ($\beta \gg 10$). It is assumed that the upstream magnetic field angle (in both regions) varied as the CIR convects from inside 1 AU to $\sim$5 AU, leading to the creation of these different layers.

[63] The trailing part of the CIR (mostly red or pink) has various layers with embedded magnetic fields, sometimes parallel and sometimes oblique. Our scenario is that when the field was parallel to the reverse shock, there would be a downstream layer generated like the bright red interval (second from the RS). This should be a HBR that has MDs.

[64] The blue region closer to the IF just beyond the pink region is meant to signify the pickup of a slow interplanetary coronal mass ejection (ICME). It will be a LBR. There should be other interplanetary phenomena embedded within the CIR layers as well.

[65] Our scenario is that CIRs at $\sim$5 AU have freshly added plasma near their shocks and also old fossil material near the IF. The plasma and fields near the IF were accumulated close to the Sun and are the oldest material within the CIR. These fossil MDs have been convected outward from the Sun without apparent further dissipation. As the CIR is convected outward, material is added at both the antisunward and sunward edges, through the FS and RS, respectively. The material adjacent and downstream of the FS and RS are the newest shock-processed material.

7. Conclusions

7.1. Are MDs Generated by the Mirror Mode Instability?

[66] This study found a lack of MD occurrence behind CIR FSs. Instead MD clusters were found in the trailing

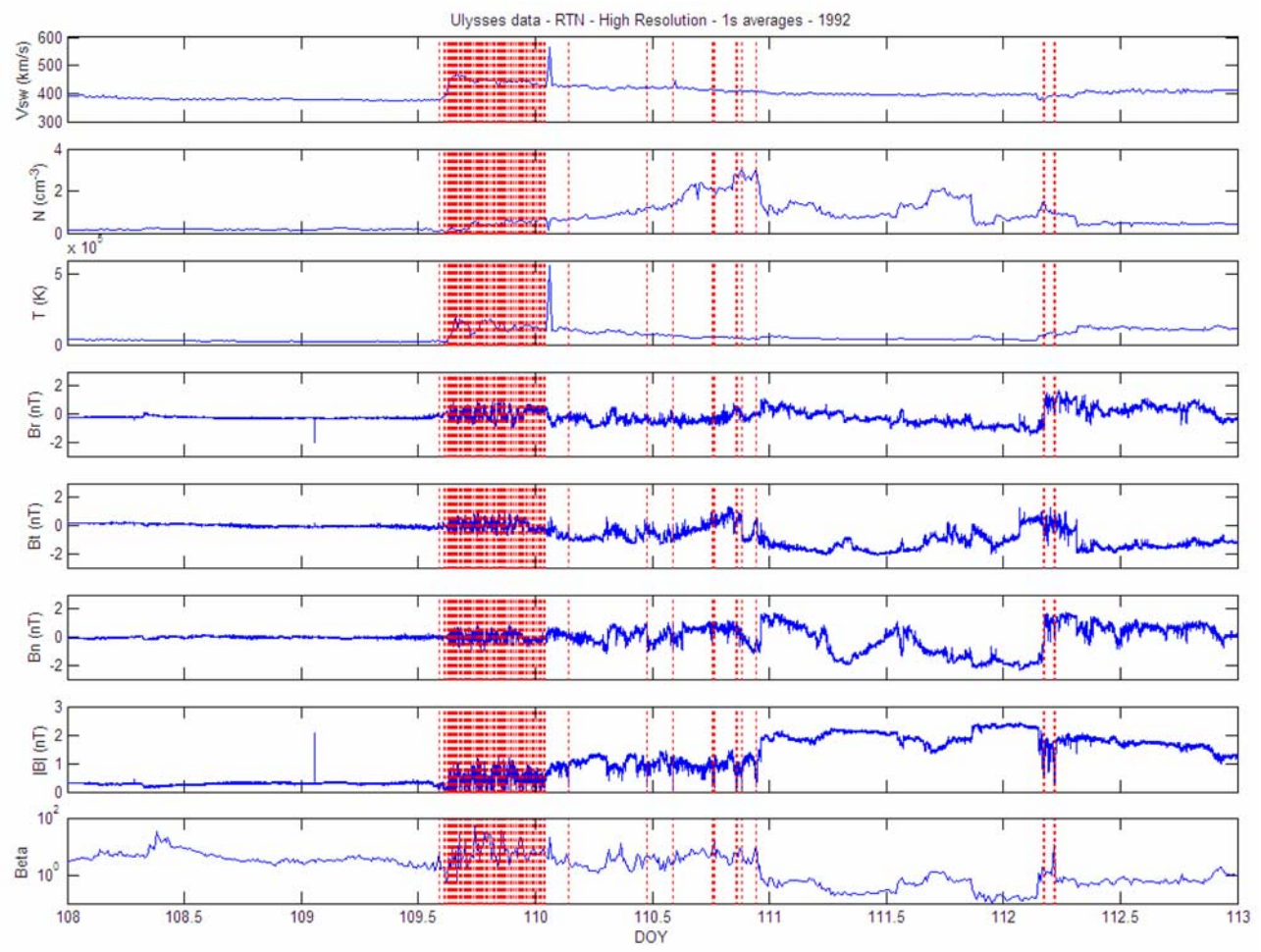

Figure 10. Same as Figure 9 but for MD event 1.

portion of CIRs downstream of the RSs. Figure 14 indicated why one would expect CIR FSs to be statistically more quasi-perpendicular than RSs. Quasi-perpendicular shocks should lead to plasma heating primarily in the direction perpendicular to the magnetic field, causing $\beta_\perp/\beta_\parallel > 1.0$ anisotropies. Thus if mirror mode generation is a source of MDs within CIRs, one would expect them to occur primarily downstream of CIR FSs, not downstream of RSs.

[67] Mirror mode structures are known to consist of a string of magnetic magnitude oscillations with little or no angular changes across the structures [*Tsurutani et al.*, 1982]. Since only a very small percentage of MDs examined in this study were found to be linear, and MDs are not detected downstream of CIR FSs, it seems unlikely that MM instability is the generation mechanism for most MDs.

7.2. Why Are Mirror Modes Not Generated Behind CIR (or ICME) FSs but Are Found in Planetary Magnetosheaths?

[68] FSs upstream of ICMEs typically have magnetosonic Mach numbers of 2–3 [*Tsurutani and Lin*, 1985]. Extremely fast ICMEs may have Mach numbers from 5–7. CIR forward shocks are typically Mach 1–4, a bit weaker (Echer et al., submitted manuscript, 2009). For the purpose of demonstration, let us assume that the upstream plasma is isotropic with $\beta = 1.0$. β has three equal components, two $\beta_\perp$ components and one $\beta_\parallel$. $\beta_\perp$ and $\beta_\parallel$ are thus both ~0.33 in the upstream region. The maximum change in the $\beta_\perp/\beta_\parallel$

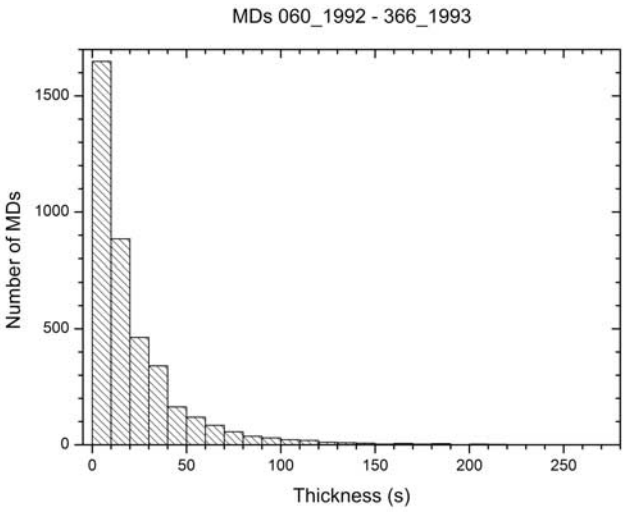

Figure 11. MD temporal thickness distribution.

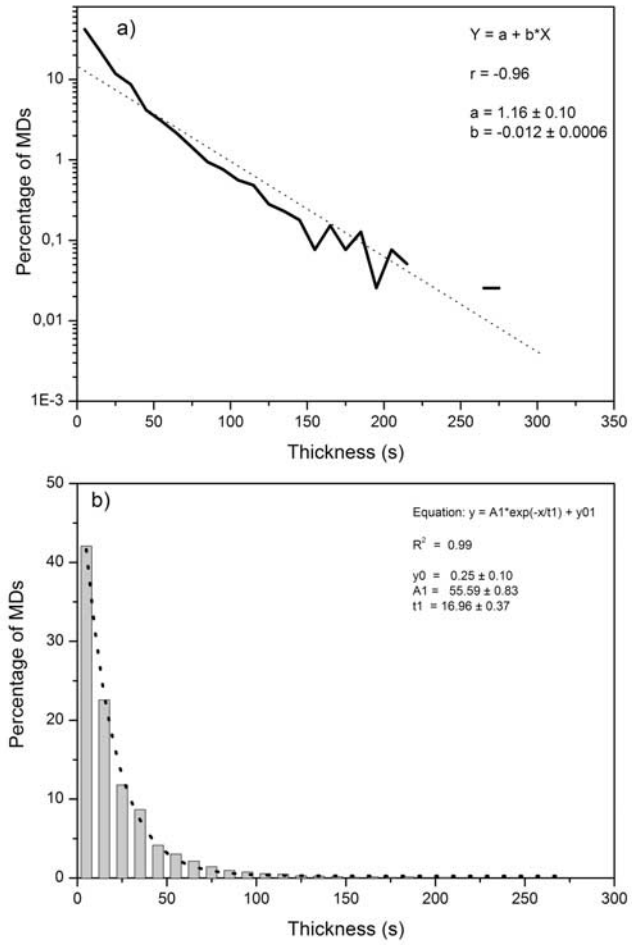

Figure 12. (a, b) Power law and exponential fits to the MD temporal thickness data.

ratio occurs across a perpendicular shock. Let us assume a perpendicular Mach 3 shock for our calculations. For this case, B_o, N, and $T_\perp$ increase by a factor of ~3 across the shock [*Kennel et al.*, 1985]. Thus $\beta_\perp$ remains unchanged

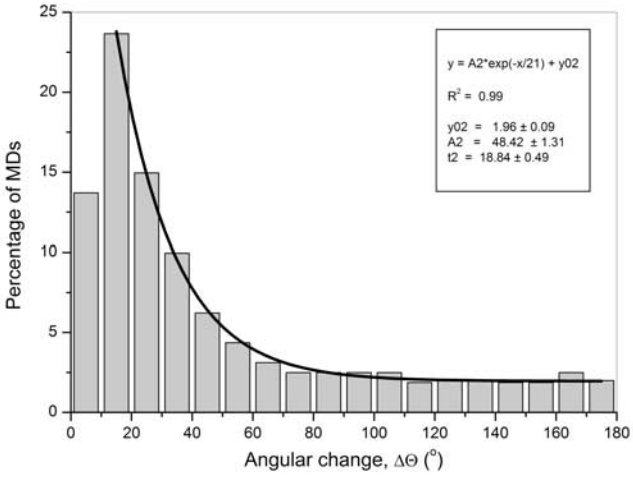

Figure 13. Magnetic field angular changes across MDs. Most MDs are not linear. The curve fit is $\%MD = 2 + 48e^{-(\Delta\Theta^\circ/18.8^\circ)}$.

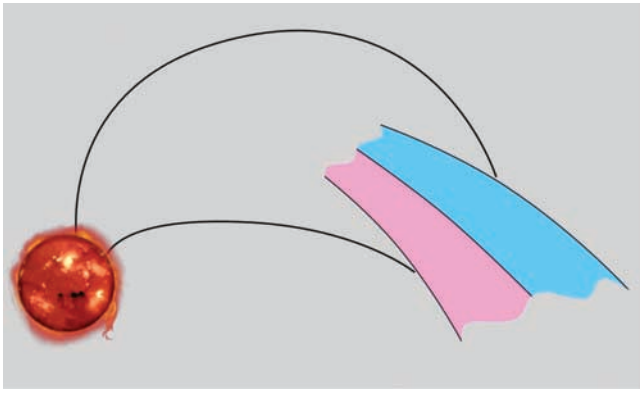

Figure 14. A schematic of a CIR far from the Sun. The magnetic field lines in the slow and fast solar winds follow the Parker configuration.

while $\beta_\parallel$ decreases by a factor of 3, giving a downstream $\beta_\perp/\beta_\parallel$ value of 3.0. This is less than the mirror mode instability criteria of $\beta_\perp/\beta_\parallel > 1 + 1/\beta_\perp = 4$.

[69] What about stronger ICME FSs? *Kennel et al.* [1985] have indicated that the maximum downstream compression factor should be ~4 independent of the strength of the shock. If this compression factor is assumed in the above calculation, it is found that in the ideal case for a purely perpendicular shock, the downstream region would be only at the threshold of instability.

[70] ICME and CIR sheaths just downstream of forward shocks should therefore be stable to MM generation. In

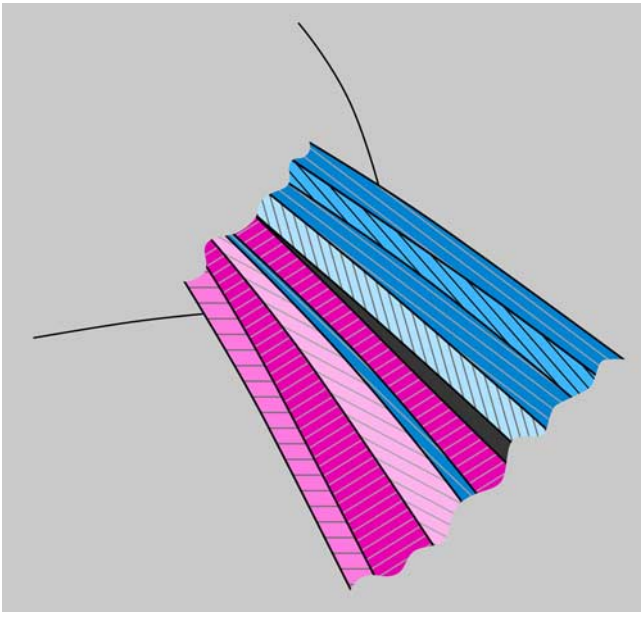

Figure 15. A detailed schematic of a CIR. The CIR is composed of multiple layers, depending on the upstream magnetic field angle to the FS and RS. If the field angle is perpendicular to the shock surface (quasi-parallel shock), the parcel of downstream plasma will be a high-plasma-β region with radial field orientations. If the angle is parallel to the shock surface, this downstream parcel will be a low-β region with orthogonal field orientations. High-β regions are indicated by pink, and low-β regions are indicated by blue.

accordance with this, there have been no observations of postshock MMs reported to date to the knowledge of the authors. We should mention that one can envision unique cases where MMs could be generated. If the upstream β were particularly high and had $\beta_\perp/\beta_\parallel > 1$ upstream anisotropies, one could expect MM generation.

[71] In planetary magnetosheaths, there is another source of free energy for mirror instability not present in CIRs. Perpendicular compression and plasma flow out from the ends of draped magnetic field lines [*Midgley and Davis*, 1963; *Zwan and Wolf*, 1976] enhances the local ion temperature anisotropy, effectively leading to further MM growth. Observationally, MM amplitudes increase continuously from the bow shock to the magnetopause, with the largest amplitudes present just outside the magnetopause (see examples by *Tsurutani et al.* [1982], *Violante et al.* [1995], and *Cattaneo et al.* [1998]). B. T. Tsurutani et al. (Mirror instability upstream of the termination shock (TS) and in planetary magnetosheaths, submitted to *Annales Geophysicae*, 2009) have speculated that it is this additional source of free energy together with quasi-perpendicular shock compression that leads to MM growth in planetary magnetosheaths, especially near the magnetopause.

[72] Besides the mirror instability, the electromagnetic ion cyclotron (EMIC) instability is also stimulated by a $T_\perp/T_\parallel > 1$ anisotropy. In fact the EMIC mode has a higher linear growth rate than does the MM instability. It has thus been a long-standing problem why MM structures are detected in planetary magnetosheaths at all. We refer the reader to the work of *Shoji et al.* [2009], who have some new insights on the competition between the growth of these two wave modes.

7.3. What Is the Cause of MDs in Clusters/Subclusters?

[73] MDs were found to occur in $1 < \beta < 10^2$ plasma regions. They were also found to occur downstream of CIR RSs and FSs with foreshocks. Of the mechanisms discussed in section 2, there are several that stand out. Compression of phase-steepened Alfvén waves [*Tsurutani et al.*, 1995, 2005a] is clearly one possibility. The high-speed stream plasma contains a higher number of nonlinear Alfvén waves than does the slow-speed stream plasma. Thus convection of these waves into the RS will enhance the wave "action" and enhance the phase-steepening process. The same argument can be used for MD event 1 with foreshock waves being convected into the shock. *Tsubouchi and Matsumoto*'s [2005] mechanism of directional discontinuity (DD) interaction with a shock (not necessarily a RS) is closely related to *Tsurutani et al.*'s [1995, 2005a] mechanism. The phase-steepened edges of Alfvén waves are DDs, and there are more DDs in high-speed streams than in slow-speed streams [*Tsurutani et al.*, 1996].

[74] *Vasquez et al.*'s [2007] concept that shock downstream turbulence creates MDs has definite merit. We have shown two examples of fast forward shocks with foreshock waves that have many MDs in the downstream sheath region (events 1 and 3). However, we note that the MDs in event 1 seemed to have a slightly different nature (not illustrated) than the MDs found downstream of CIR RSs. How do high-β plasmas lead to MDs? The model also does not provide any answer to this question.

[75] Numerical simulations with a 3-D hybrid code could perhaps answer some or all of these questions. We encourage interested parties to do realistic modeling of Alfvén wave and or DD interactions with quasi-parallel shocks to investigate downstream results.

8. Final Comments

[76] We have approached the discussion of MD generation during the Ulysses first fast latitude scan with an assumption that there is one mechanism that is generating all or most of the events. This approach has the advantage that a scenario is provided which can be tested in the future.

[77] It is clear that there are circumstances where other mechanisms are operative and the MD generation picture becomes more complex. For example a small number of mirror mode structures (as well as steepened Alfvén waves) have been previously noted in a CIR [*Tsurutani et al.*, 1995]. So certainly at times this mechanism can be operative in interplanetary space. It was noted that the MDs downstream of the event 1 quasi-parallel FS might be somewhat different than other MDs (this effort was beyond the scope of the present work). If this is true, then MD generation by wave-wave interactions [*Vasquez et al.*, 2007] may be the source of this MD cluster. There are also MDs that occur in the high-speed stream proper (albeit at a very low occurrence rate). Clearly these are not related to shock interactions.

[78] The presence of MD clusters in interplanetary space shows that the medium can be highly compressive. How this influences energetic particle propagation through the heliosphere is an open question and merits detailed computer simulations.

[79] **Acknowledgments.** Portions of the research were performed at the Jet Propulsion Laboratory, California Institute of Technology, under contract with NASA. E.E. wishes to thank the CNPq agency for financial support (contracts PQ-300014/2005–7 and 470406/2006–8). G.S.L. thanks the Indian National Science Academy, New Delhi, for support under the Senior Scientist Scheme. F.L.G. and B.T.T. would like to thank FAPESP for support through project 2008/05607–2.

[80] Zuyin Pu thanks the reviewer for assistance in evaluating this paper.

References

Abraham-Shrauner, B. (1972), Determination of magnetohydrodynamic shock normals, *J. Geophys. Res.*, *77*, 736, doi:10.1029/JA077i004p00736.

Bame, S. J., B. E. Goldstein, J. T. Gosling, J. W. Harvey, D. J. McComas, M. Neugebauer, and J. L. Phillips (1993), Ulysses observations of a recurrent high speed solar wind stream and the heliomagnetic streamer belt, *Geophys. Res. Lett.*, *20*, 2323, doi:10.1029/93GL02630.

Baumgärtel, K. (1999), Soliton approach to magnetic holes, *J. Geophys. Res.*, *104*, 28,295, doi:10.1029/1999JA900393.

Brinca, A. L., and B. T. Tsurutani (1988), Survey of low frequency electromagnetic waves stimulated by two coexisting newborn ion species, *J. Geophys. Res.*, *93*, 48, doi:10.1029/JA093iA01p00048.

Burlaga, L. F., and J. F. Lemaire (1978), Interplanetary magnetic holes: Theory, *J. Geophys. Res.*, *83*, 5157, doi:10.1029/JA083iA11p05157.

Buti, B., B. T. Tsurutani, M. Neugebauer, and B. E. Goldstein (2001), Generation mechanism for magnetic holes in the solar wind, *Geophys. Res. Lett.*, *28*, 1355, doi:10.1029/2000GL012592.

Cattaneo, M. B. B., C. Basile, G. Moreno, and J. D. Richardson (1998), Evolution of mirror structures in the magnetosheath of Saturn from the bow shock to the magnetopause, *J. Geophys. Res.*, *103*, 11,961, doi:10.1029/97JA03683.

Chandrasekhar, S. A., A. N. Kaufman, and K. M. Watson (1958), The stability of the pinch, *Proc. R. Soc. London, Ser. A*, *245*, 435, doi:10.1098/rspa.1958.0094.

Dasgupta, B., B. T. Tsurutani, and M. S. Janaki (2003), A kinetic approach to the Ponderomotive Force, *Geophys. Res. Lett.*, *30*(21), 2128, doi:10.1029/2003GL017385.

Fränz, M., D. Burgess, and T. S. Horbury (2000), Magnetic depressions in the solar wind, *J. Geophys. Res.*, *105*, 12,725, doi:10.1029/2000JA900026.

Gonzalez-Esparza, J. A., E. J. Smith, A. Balogh, and J. L. Phillips (1996), The quasi-parallel shock wave detected by Ulysses on day 92:109, *Astron. Astrophys.*, *316*, 323.

Guarnieri, F. L., B. T. Tsurutani, and E. Echer (2009), The interplanetary magnetic decrease automatic detection (IMDAD) code, *Earth Planets Space*, *61*, 585.

Hasegawa, A. (1969), Drift mirror instability in the magnetosphere, *Phys. Fluids*, *12*, 2642, doi:10.1063/1.1692407.

Hasegawa, A. (1975), *Plasma Instabilities and Nonlinear Effects*, *Phys. Chem. Space*, vol. 8, 94 pp., Springer, New York.

Kennel, C. F., J. P. Edmiston, and T. Hada (1985), A quarter century of collisionless shock research, in *Collisionless Shocks in the Heliosphere: A Tutorial Review*, *Geophys. Monogr. Ser.*, vol. 34, edited by R. G. Stone and B. T. Tsurutani, p. 1, AGU, Washington, D. C.

Kennel, C., et al. (1988), Nonlinear, dispersive, elliptically polarized Alfvén waves, *Phys. Fluids*, *31*, 1949, doi:10.1063/1.866642.

Midgley, J. E., and L. Davis Jr. (1963), Calculation by a moment technique of the perturbation of the geomagnetic field by the solar wind, *J. Geophys. Res.*, *68*, 5111.

Neugebauer, M., B. E. Goldstein, D. Winterhalter, E. J. Smith, R. J. McDowell, and S. P. Gary (2001), Ion distribution in large magnetic holes in the fast solar wind, *J. Geophys. Res.*, *106*, 5635, doi:10.1029/2000JA000331.

Pizzo, V. J. (1985), Interplanetary shocks on the large scale: A retrospective on the last decade's theoretical efforts, in *Collisionless Shocks in the Heliosphere: Reviews of Current Research*, *Geophys. Monogr. Ser.*, vol. 35, edited by B. T. Tsurutani and R. G. Stone, pp. 51–68, AGU, Washington, D. C.

Pokhotelov, O. A., R. Z. Sagdeev, M. A. Balikhin, and R. A. Treumann (2004), Mirror instability at finite ion-Larmor radius wavelengths, *J. Geophys. Res.*, *109*, A09213, doi:10.1029/2004JA010568.

Pokhotelov, O. A., R. Z. Sagdeev, M. A. Balikhin, and R. A. Treumann (2005), Comment on "Theory and observations of slow-mode solitons in space plasmas", *Phys. Rev. Lett.*, *95*, 129501, doi:10.1103/PhysRevLett.95.129501.

Price, C. P., D. W. Swift, and L.-C. Lee (1986), Numerical simulation of nonoscillatory mirror mode waves at the Earth's magnetosheath, *J. Geophys. Res.*, *91*, 101, doi:10.1029/JA091iA01p00101.

Shoji, M., et al. (2009), Mirror instability and L mode electromagnetic ion cyclotron instability: Competition in the Earth's magnetosheath , *J. Geophys. Res.*, doi:10.1029/2008JA014038, in press.

Smith, E. J., B. T. Tsurutani, and R. L. Rosenberg (1978), Observations of the interplanetary sector structure up to heliographic latitudes of 16°: Pioneer 11, *J. Geophys. Res.*, *83*, 717, doi:10.1029/JA083iA02p00717.

Smith, E. J., M. Neugebauer, A. Balogh, S. J. Bame, G. Erdos, R. J. Forsyth, B. E. Goldstein, J. L. Phillips, and B. T. Tsurutani (1993), Disappearance of the heliospheric sector structure at Ulysses, *Geophys. Res. Lett.*, *20*, 2327, doi:10.1029/93GL02632.

Stevens, M. L., and J. C. Kasper (2007), A scale-free analysis of magnetic holes at 1 AU, *J. Geophys. Res.*, *112*, A05109, doi:10.1029/2006JA012116.

Tsubouchi, K. (2007), Alfvén wave evolution in an interaction system of the fast and slow solar wind, *Eos Trans. AGU*, *88*(52), Fall Meet. Suppl., Abstract SH22A-0848.

Tsubouchi, K., and H. Matsumoto (2005), Effect of upstream rotational field on the formation of magnetic depressions in a quasi-perpendicular shock downstream, *J. Geophys. Res.*, *110*, A04101, doi:10.1029/2004JA010818.

Tsurutani, B. T., and C. M. Ho (1999), A review of discontinuities and Alfvén waves in interplanetary space: Ulysses results, *Rev. Geophys.*, *37*, 517, doi:10.1029/1999RG900010.

Tsurutani, B. T., and R. P. Lin (1985), Acceleration of >47 keV ions and >2 keV electrons by interplanetary shocks at 1 AU, *J. Geophys. Res.*, *90*, 1, doi:10.1029/JA090iA01p00001.

Tsurutani, B. T., E. J. Smith, R. R. Anderson, K. W. Ogilvie, J. D. Scudder, D. N. Baker, and S. J. Bame (1982), Lion roars and nonoscillatory drift mirror waves in the magnetosheath, *J. Geophys. Res.*, *87*, 6060, doi:10.1029/JA087iA08p06060.

Tsurutani, B. T., C. M. Ho, E. J. Smith, M. Neugebauer, B. E. Goldstein, J. S. Mok, J. K. Arballo, A. Balogh, D. J. Southwood, and W. C. Feldman (1994), The relationship between interplanetary discontinuities and Alfvén waves: Ulysses observations, *Geophys. Res. Lett.*, *21*, 2267, doi:10.1029/94GL02194.

Tsurutani, B. T., C. M. Ho, J. K. Arballo, B. E. Goldstein, and A. Balogh (1995), Large amplitude IMF fluctuations in corotating interaction regions: Ulysses at midlatitudes, *Geophys. Res. Lett.*, *22*, 3397, doi:10.1029/95GL03179.

Tsurutani, B. T., C. M. Ho, J. K. Arballo, E. J. Smith, B. E. Goldstein, M. Neugebauer, A. Balogh, and W. C. Feldman (1996), Interplanetary discontinuities and Alfvén waves at high heliographic latitudes: Ulysses, *J. Geophys. Res.*, *101*, 11,027, doi:10.1029/95JA03479.

Tsurutani, B. T., G. S. Lakhina, E. J. Smith, B. Buti, S. L. Moses, F. V. Coroniti, A. L. Brinca, J. A. Slavin, and R. D. Zwickl (1999), Mirror mode structures and ELF plasma waves in the Giacobini-Zinner magnetosheath, *Nonlinear Processes Geophys.*, *6*, 229.

Tsurutani, B. T., B. Dasgupta, C. Galvan, M. Neugebauer, G. S. Lakhina, J. K. Arballo, D. Winterhalter, B. E. Goldstein, and B. Buti (2002a), Phase-steepened Alfvén waves, proton perpendicular energization and creation of magnetic holes and magnetic decreases: The ponderomotive force, *Geophys. Res. Lett.*, *29*(24), 2233, doi:10.1029/2002GL015652.

Tsurutani, B. T., C. Galvan, J. K. Arballo, D. Winterhalter, R. Sakurai, E. J. Smith, B. Buti, G. S. Lakhina, and A. Balogh (2002b), Relationship between discontinuities, magnetic holes, magnetic decreases, and nonlinear Alfvén waves: Ulysses observations over the solar poles, *Geophys. Res. Lett.*, *29*(11), 1528, doi:10.1029/2001GL013623.

Tsurutani, B. T., B. Dasgupta, J. K. Arballo, G. S. Lakhina, and J. S. Pickett (2003), Magnetic field turbulence, electron heating, magnetic holes, proton cyclotron waves and the onset of bipolar pulses (electron hole) events: A possible unifying scenario, *Nonlinear Processes Geophys.*, *10*, 27.

Tsurutani, B. T., G. S. Lakhina, J. S. Pickett, F. L. Guarnieri, N. Lin, and B. E. Goldstein (2005a), Nonlinear Alfvén waves, discontinuities, proton perpendicular acceleration, and magnetic holes/decreases in interplanetary space and the magnetosphere: Intermediate shocks?, *Nonlinear Processes Geophys.*, *12*, 321.

Tsurutani, B. T., F. L. Guarnieri, G. S. Lakhina, and T. Hada (2005b), Rapid evolution of magnetic decreases (MDs) and discontinuities in the solar wind: ACE and CLUSTER, *Geophys. Res. Lett.*, *32*, L10103, doi:10.1029/2004GL022151.

Turner, J. M., L. F. Burlaga, N. F. Ness, and J. F. Lemaire (1977), Magnetic holes in the solar wind, *J. Geophys. Res.*, *82*, 1921, doi:10.1029/JA082i013p01921.

Vasquez, B. J., V. I. Abramenko, D. K. Haggerty, and C. W. Smith (2007), Numerous small magnetic field discontinuities of Bartels rotation 2286 and the potential role of Alfvénic turbulence, *J. Geophys. Res.*, *112*, A11102, doi:10.1029/2007JA012504.

Violante, L., B. M. B. Cattaneo, G. Moreno, and J. D. Richardson (1995), Observations of mirror waves and plasma depletion layer upstream of Saturn's magnetopause, *J. Geophys. Res.*, *100*, 12,047, doi:10.1029/94JA02703.

Winterhalter, D., M. Neugebauer, B. E. Goldstein, E. J. Smith, S. J. Bame, and A. Balogh (1994), Ulysses field and plasma observations of magnetic holes in the solar wind and their relation to mirror-mode structures, *J. Geophys. Res.*, *99*, 23,371, doi:10.1029/94JA01977.

Winterhalter, D., M. Neugebauer, B. E. Goldstein, E. J. Smith, B. T. Tsurutani, S. J. Bame, and A. Balogh (1995), Magnetic holes in the solar wind and their relation to mirror-mode structures, *Space Sci. Rev.*, *72*, 201, doi:10.1007/BF00768780.

Winterhalter, D., E. J. Smith, M. Neugebauer, B. E. Goldstein, and B. T. Tsurutani (2000), The latitudinal distribution of solar wind magnetic holes, *Geophys. Res. Lett.*, *27*, 1615, doi:10.1029/1999GL003717.

Zwan, B. J., and R. A. Wolf (1976), Depletion of the solar wind plasma near a planetary boundary, *J. Geophys. Res.*, *81*, 1636, doi:10.1029/JA081i010p01636.

E. Echer, Instituto Nacional Pesquisas Espaciais, 12227 São Paulo, Brazil.

F. L. Guarnieri, Instituto de Pesquisa e Desenvolvimento, Universidade do Vale do Paraíba, Avenida Shishima Hifumi, 2911, CEP 12244-000, São José dos Campos SP, Brazil.

G. S. Lakhina, Indian Institute of Geomagnetism, Plot 5, Sector 18, Kalamboli Highway, Panvel (W), Navi Mumbai-410 218, India. (lakhina@iigs.iigm.res.in)

B. T. Tsurutani and O. P. Verkhoglyadova, Jet Propulsion Laboratory, California Institute of Technology, 4800 Oak Grove Drive, Pasadena, CA 91109, USA. (bruce.t.tsurutani@jpl.nasa.gov)